A REVIEW OF FLOW DIAGNOSTIC METHODS AND APPLICATIONS

A Paper
Submitted to the Graduate Faculty
of the
North Dakota State University
of Agriculture and Applied Science

By

Matthewscott Davidbryan Dale

In Partial Fulfillment of the Requirements
for the Degree of
MASTER OF SCIENCE

Major Department:
Mechanical Engineering

April 2023

Fargo, North Dakota

North Dakota State University
Graduate School

Title

A REVIEW OF FLOW DIAGNOSTIC METHODS AND APPLICATIONS

By

Matthewscott Davidbryan Dale

The Supervisory Committee certifies that this ***disquisition*** complies with North Dakota State University's regulations and meets the accepted standards for the degree of

MASTER OF SCIENCE

SUPERVISORY COMMITTEE:

Jordi Estevadeordal
Chair

Yildirim Suzen

Alan Denton

Approved:

4/13/2023
Date

Chad Ulven
Department Chair

ABSTRACT

This work provides an overview of common flow velocimetry and diagnostic techniques, including their working principles and the application of these techniques. Probe velocimetry techniques such as pitot tubes and hot wire anemometry are discussed along with unintrusive techniques such as Laser Doppler Velocimetry and Particle Image Velocimetry. Density, pressure, and temperature diagnostic methods are also examined, in particular shadowgraph/schlieren imaging, pressure/temperature sensitive paints, and infrared thermography. Benefits and drawbacks of each method are examined as well as the applications. The goal of this review is to provide the reader with a basic understanding of the methods discussed, as well as to give insight as to which methods are particularly useful and applicable to engineering measurements.

ACKNOWLEDGMENTS

I would like to extend an immense amount of gratitude to my advisor, Dr. Estevadeordal, for his understanding and support in the completion of this project. I would also like to thank Dr. Suzen and Dr. Denton for being supportive members of my graduate committee as well as a thank you to the North Dakota State University Mechanical Engineering Department for giving me the opportunity to further my education in this field of study.

TABLE OF CONTENTS

LIST OF FIGURES

LIST OF SYMBOLS

a.....Speed of Sound

C.....Tracing Particle Frequency Response

d_p.....Tracing Particle Diameter

E_w.....Hot Wire Voltage

f_D.....Doppler Frequency Shift

F.....Force

g.....Acceleration due to gravity

h.....Height of fluid

I.....Electric Current (2.2), Light Intensity (3.1)

k.....Thermal Conductivity

K.....Gladstone-Dale Coefficient

Kn.....Knudsen Number

L.....Length from test region to reference plane

L_w.....Hot Wire Length

M.....Mach Number

n.....Refractive Index

n_o.....Refractive index of surrounding fluid

Nu.....Nusselt Number

P.....Static Pressure

P_o.....Stagnation Pressure

R.....Specific Gas Constant

R_a.....Resistance of Ambient Temperature

R_w.....Resistance of Hot Wire

St.....Stokes Number

T_a .....Ambient Temperature

T_o .....Stagnation Temperature

T_w .....Hot Wire Temperature

U.....Effective Velocity of Hot Wire

U_p .....Tracing Particle Velocity

V.....Fluid Velocity

$\hat{V}$ .....Tracing Particle Lag

α .....Angle between observed and incident rays

α_o .....Coefficient of Resistance at Ambient Temperature

β .....Bisector angle of observed and incident rays

γ.....Specific Heat Ratio

μ_f .....Dynamic viscosity of fluid

ε.....Ray Deflection Angle

Θ.....Angle between dual lasers

θ_1 .....Angle of Incidence

θ_2 .....Angle of Refraction

λ.....Light Wavelength

ρ.....Density

ρ_p .....Tracing Particel Density

τ_f .....Fluid Reaction Time

τ_p.....Particle Relaxation Time

1. INTRODUCTION

Flow diagnostics is the measurement of properties of a flow field or flow phenomena in order to quantify and/or visualize the flow at a particular point or over a continuous test section. Velocity measurements, known as velocimetry, utilize various properties of flow to either indirectly measure the velocity, such as in pitot tubes, hot wire anemometry, or laser doppler velocimetry, or to directly measure the velocity through use of particle image velocimetry. The variance in measurement methods of these techniques, namely the determination of dynamic pressure, resistance change, wavelength doppler shift, and total particle displacement, respectively, result in each method having ideal and unideal conditions which to measure flow, as well as varying accuracy and precision of such measurements. Density and density gradients are also common properties of flow that can be visualized qualitatively using shadowgraph and schlieren techniques. Images produced from these methods clearly show the location of density gradients in a flow field which is useful particularly for identifying thermal fields and shock wave locations. Pressure and temperature distributions on a body are essential in determining the loading of forces as well as verifying computational fluid dynamics (CFD) simulations. Quantitative measurement of pressure and temperature on a body have been traditionally done with point source measurements, such as static pressure ports and thermocouples. Spatial analysis of these properties, however, can be measured using techniques such as pressure and temperature sensitive paints or infrared thermography, both of which provide high accuracy analysis of the pressure and/or temperature distributions over a body. This work reviews these techniques, both their working principles and their applications in fluid dynamics research.

2. VELOCIMETRY TECHNIQUES

2.1. Pitot Tubes

One of the earliest and simplest ways to measure fluid velocity is through use of a Pitot Tube. Pitot Tubes operate by measuring both the static pressure of a fluid through static ports as well as the stagnation pressure, or the pressure of the fluid flow when brought to a full stop as seen in figure 1. Subtracting the static pressure from the stagnation pressure gives the dynamic pressure, and through simple manipulation of Bernoulli's equation shown in Equation 1 and 2, the velocity of the flow can be calculated. This method of calculating the velocity requires incompressible fluids to be measured, such as liquids or gases with a velocity of less than Mach 0.3. Gasses travelling any faster are considered compressible which causes a change in density that results in error if the constant density assumption in Bernoulli's equation is used [1].

$$p_1 + \frac{1}{2}\rho V_1^2 + \rho g h_1 = p_2 + \frac{1}{2}\rho V_2^2 + \rho g h_2 \quad \textbf{(1)}$$

$$V_1 = \sqrt[2]{\frac{2(p_o - p_1)}{\rho}} \quad \textbf{(2)}$$

Where p is static pressure, ρ is fluid density, V is flow velocity, g is acceleration due to gravity, h is height of the fluid, and p_o is stagnation pressure. For compressible flows, isentropic relations must be used in order to calculate the true flow velocity. As seen in equation 3, the stagnation pressure static pressure ratio can be manipulated to solve for the Mach number, M, of subsonic compressible flow if the specific heat ratio, γ, is known. Flow velocity can be calculated using equation 4 which requires knowledge of the stagnation temperature T_o and the specific gas constant R, with 'a' being the speed of sound in the particular fluid [1].

$$\frac{p_o}{p} = \left(1 + \frac{\gamma - 1}{2} M^2\right)^{\gamma/(\gamma-1)} \quad \textbf{(3)}$$

$$V^2 = a^2 M^2 = \frac{\gamma R T_o M^2}{1 + \frac{\gamma - 1}{2} M^2} \quad \textbf{(4)}$$

Supersonic flows will cause a bow shock to form in front of the pitot tube, so the directly measured static and stagnation pressures will not be that of the true flow velocity. Normal shock relations can be used to solve for the Mach number before the bow shock as seen in equation 5 [1].

$$\frac{p_{o2}}{p_1} = \frac{p_{o2}}{p_2}\frac{p_2}{p_1} = \left(\frac{(\gamma+1)^2 M_1^2}{4\gamma M_1^2 - 2(\gamma - 1)}\right)^{\gamma/(\gamma-1)} \frac{1 - \gamma + 2\gamma M_1^2}{\gamma + 1} \quad \textbf{(5)}$$

Pitot tubes are widely used on aircrafts for measurement of the vehicle's local airspeed and Mach number. Due to the ease of use and wide availability of pitot tubes, they are often used in measuring airflow in ducts and for measurement of wind speed for weather reporting. However, the invasive nature, low frequency response, and the necessity to be relatively parallel to the flow direction to give the true velocity measurement limits the use of pitot tubes in complex flow field measurements.

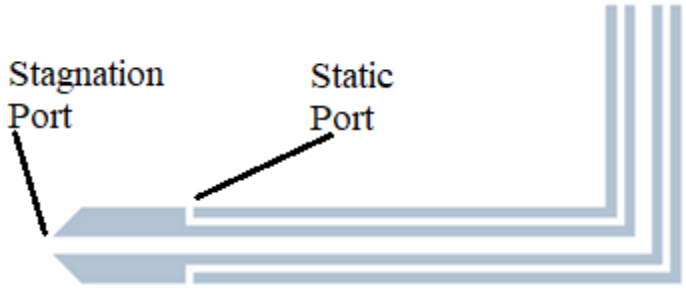

Figure 1. Pitot Tube with static pressure port

2.2. Hot Wire Anemometry

Hot Wire Anemometry (HWA) is another intrusive diagnostic technique due to the insertion of a probe and its mounting equipment into the flow used to measure flow velocity and fluctuations. The working principle of this method is to place a small wire with flowing electric current into a flow field. Forced convection cools the wire as the fluid moves over it, slightly changing the resistance of the wire which can be measured with circuits such as a Wheatstone bridge. This change in resistance is used to calculate the cooling effects on the wire, and using the convection equation, the flow velocity can be calculated [2]. Due to the small size of the wire used, hot wire techniques have much less of an effect on the flow field than a pitot tube. The frequency of the hot wire techniques is also on the scale of kHz, giving very accurate velocity data and allowing for more accurate analysis of turbulent flow fluctuations [3]. However, while a three-component hot wire system is possible, poor spatial resolution and lack of flow reversal detection restrict its utility. And while HWA has a higher frequency response and smaller size than a pitot tube, its presence in a supersonic flow field will still result in, besides fragility, bow shock formation, limiting its utility in high-speed flow [3].

There are three main methods of HWA, constant current, constant temperature, and constant voltage. Due to its widespread use and utility in high frequency/amplitude fluctuating flows, constant temperature anemometry (CTA) circuit design and signal processing will be the focus of this section. The sensor portion of a hot wire anemometer is made up of a thin wire in the range of 1 to 5 μm in diameter and .1 to 3mm in length. Common wire materials are platinum, tungsten, or platinum-iridium, and the wire itself is connected to prongs that pass current through it as well as hold up the wire as fluid flows over it. Coating can be added to the

outer lengths of the wire close to the prongs to reduce length of wire actually being cooled, improving the overall spatial resolution of the HWA system [4].

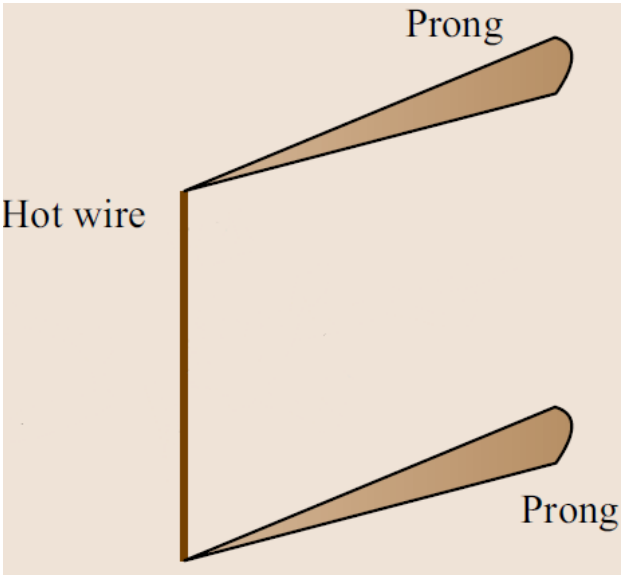

Figure 2. Diagram of hot wire sensor [2]

Resistance of a hot wire with respect to its temperature can be approximated by the linearized relation in equation 6, where R_w is the resistance measured by the wire, R_a is the wire resistance at ambient temperature, α_o is the coefficient of resistivity at ambient temperature, T_w is temperature of the wire, and T_a is the ambient temperature [5].

$$R_w = R_a[1 + \alpha_o(T_w - T_a)] \quad \textbf{(6)}$$

By assuming a steady state system, the power output, i.e., heating of the wire can be equated to the forced convective cooling due to fluid flow. By substituting the convection coefficient in terms of the Nusselt number, Nu, the Joule heating of the wire can be expressed as seen in equation 7, with L_w representing the wire length, k representing the wire material thermal conductivity, and I representing the current through the wire.

$$I^2 R_w = \pi L_w k (T_w - T_a) Nu \quad \textbf{(7)}$$

King's law can be applied to equation 7 to approximate the Nusselt number through a power law relation, with A and B being constant coefficients. Additional modification can be made to equation 8 to relate the King's law directly to the square of the output voltage, E_w, allowing for a simple power law relation between the voltage and effective velocity, U. The exponential "n" can be approximated in the range of .45-.5 but can also be simultaneously solved along with A and B for more accurate curve fitting and velocity measurements [5].

$$\frac{E_W^2}{R_W} = (A + BU^n)(T_w - T_o) \quad \textbf{(8)}$$

The circuit design of CTA consists of a Wheatstone bridge and a voltage amplifier seen in figure 3. The Wheatstone bridge begins in a balanced state, and as the fluid flows over the sensor wire, the resistance changes and voltage is detected by the amplifier as the bridge is now unbalanced. Current is generated by the circuit to balance the bridge and keep the wire at a constant temperature, and the voltage change can be measured and processed to calculate velocity fluctuations and mean velocity over the sensor.

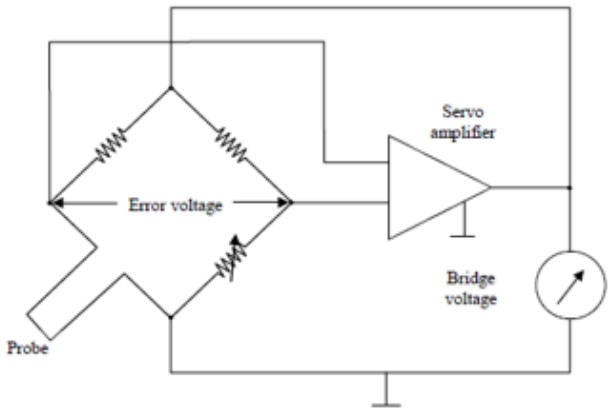

Figure 3. Wheatstone bridge diagram [2]

Calibration of an HWA setup for subsonic flows can be done by linearly relating the square velocity of a wind tunnel from a pitot tube to the voltage measured by the hot wire to the .45 power. This linear relation is the essence of King's Law and will give the A and B coefficients. Alternatively, the velocity and voltage measurements can be compared directly using a power curve fit to approximate the relationship between the quantities. An example of this type of curve fitting is seen in figure 4.

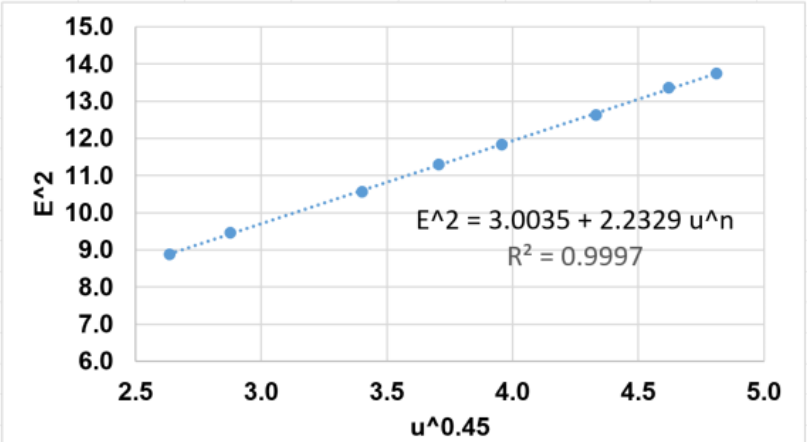

Figure 4. Calibration curve for subsonic HWA
REF: ME 478/678 Advanced Fluid Diagnostics

Single wire HWA setups are only capable of measuring effective fluid velocity in one direction. With additional wires, 2D and 3D analysis of fluid flow can be processed. Adding wires to a HWA setup orthogonal to each other will allow for the calculation of velocity components in different dimensions, with a three wire setup capable of measuring all 3 velocity components. However, because the wires themselves must be separated, there is spatial error as the measurement points are not in the same place. Lack of directionality of the wires also prevents HWA from finding the full velocity vectors at a point [5].

2.3. Laser Doppler Velocimetry

Laser Doppler Velocimetry (LDV) is a common velocimetry method that allows for point measurements of velocity components in a flow field. Two laser beams intersect at a particular angle, producing a volume where tracing particles can pass through and scatter the incoming light. The Doppler effect causes the scattered light to have a slightly shifted frequency which can be measured and used to determine the velocity of the tracing particles, and therefore the flow field at the chosen point. LDV provides several benefits over other point velocity measurement techniques such as pitot tubes and HWA, mainly its minimal effect on the flow dynamics of a system, its very high spatial and temporal resolution, as well as its high accuracy due to the fact that traditional calibration techniques are not required. LDV can also remove directional ambiguity in its measurements, unlike HWA [6].

The main principle utilized by LDV measurements is the Doppler effect of light due to the scattering of light off of moving particles. An incident beam of frequency f will hit and scatter off of a moving particle with a shifted frequency. The shift in frequency, f_D, is determined by the bisector angle between the incident and observed light beams, β, the angle between the continued incident beam and the observed beam, α, inversely proportional to the wavelength, λ, of the incident beam, and directly proportional to the velocity of the particle scattering the light, as shown in equation 9 [2]. A visualization of these angles for determining the Doppler shift is shown in figure 5. Once the shift in frequency is known, the velocity component can be determined. However, direct measurement of f_D is very difficult as the shift is typically extremely small, usually in the MHz range, compared to the frequency of light being used, usually 10^{15} Hz. For LDV applications, indirect measurement techniques are typically utilized in order to determine the doppler shift [6].

$$f_d = \frac{2V}{\lambda}\cos(\beta)\sin\left(\frac{\alpha}{2}\right) \quad \textbf{(9)}$$

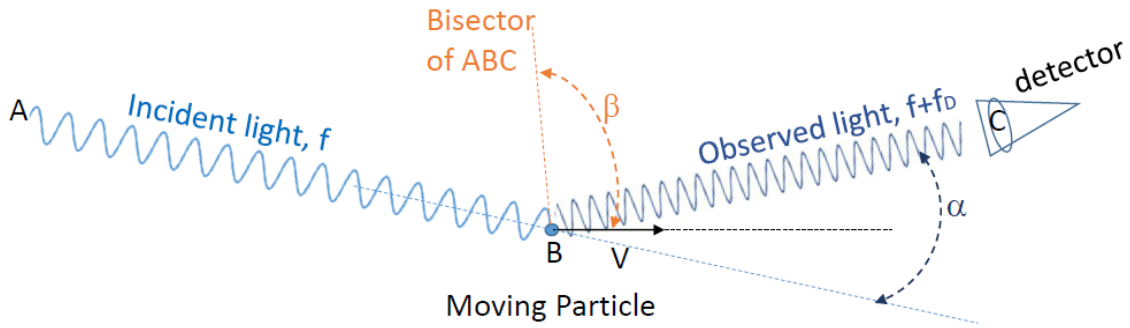

Figure 5. Diagram of Doppler shift due to particle motion
REF: ME 478/678 Advanced Fluid Diagnostics

The most common method of indirectly measuring this shift is by intersecting two laser beams at a point to create a small volume of measurement at which tracer particles pass through and scatter light from the two beams. The orientation of the two beams will cause the frequency of light scattered from them to be slightly different from each other. The absolute difference in frequency between these two beams is equivalent to f_D, and equation 10 can be derived and used to relate f_D to the angle between the incident beams, incident beam wavelength, and perpendicular velocity component only. The difference between the shifted frequencies can be found by heterodyning the two frequencies, f_1 and f_2, and measuring the beat frequency of the signal, which is equivalent to f_D. The measurement of the beat frequency gives this method, the beat frequency method, its name. Because the incident beam wavelength and angle between the incident beams, Θ, can be accurately measured, traditional calibration techniques done with HWA are not required for LDV setups [6].

$$f_D = f_1 - f_2 = +\frac{2\sin\frac{\Theta}{2}}{\lambda}V \quad \textbf{(10)}$$

Alternative to beat frequency mixing, the fringe pattern method can be used to determine the doppler shift frequency and find the velocity component of tracing particles. At the intersection of the two laser beams, constructive and destructive interference of the light waves will cause interference fringes to form as seen in figure 6. The distance between fringes can be expressed as seen in equation 11 [2]. As particles pass through the fringe pattern, the frequency of the light bursts is equivalent to f_D. The velocity component is then calculated from this measured frequency. In order to remove directional ambiguity from LDV measurements, it is necessary to slightly shift one of the laser beam's frequencies in order to cause the fringe interference pattern to begin to move. This shift in frequency, f_S, allows for the detection of particles with no velocity, resulting in a measured frequency of f_S. Tracer particles traveling in the "negative" direction, or direction of the moving fringes, will be directionally unambiguous assuming their velocity doesn't exceed the velocity of the moving fringes.

$$s = \frac{\lambda}{2 \sin \frac{\theta}{2}} \tag{11}$$

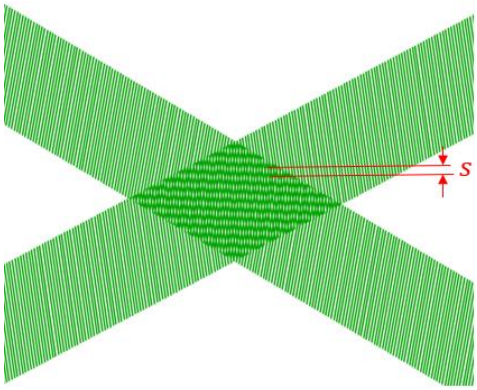

Figure 6. Fringe pattern at intersection of laser beams
REF: ME 478/678 Advanced Fluid Diagnostics

LDV setups allow for a great deal of freedom and variety of where and how transmitters and receivers are set up. Because the scattering of light off of the tracing particles goes in all

directions, as long as photodetectors are close and not obstructed, they can be placed at any angle to the incident beams. However, light intensity of this scattering is strongest in the forward direction of the beams, so placement of detecting optics opposite of transmitting equipment will result in the best signal strength [2]. Consolidation of transmitting and receiving optics into the same component allows for simpler setups but reduces signal strength as backscattered light is being detected. Bragg cells are typically used to not only split incident beams into two, but to also slightly shift the frequency of one of those beams through acoustic diffraction. If a two-color incident beam is utilized, a color splitter can allow for further splitting of the incident beams. Orienting these beam pairs orthogonal to each other allows for the detection of two components of the tracer particle velocity rather than just one. A third beam pair with a different frequency to the first two can then be oriented to allow for 3D velocity measurements of a tracer particle. The different frequencies of the beams allow the light pulses of each fringe pattern to be distinguished from one another so the proper Doppler shifts can be measured, and velocity components calculated [7].

The spatial and temporal resolutions of LDV are high and allow for precise determination of the velocity component of flow at a particular point. The intersection of the two laser beams creates an ellipsoidal volume that tracer particles pass through for detection. The exact volume of this ellipsoid is determined by the diameter of the beam waist from the Gaussian laser beam as well as the angle between the incident beams. The diameter of this volume will have a typical range between 40 μm and 200 μm, with a length approximately 5 to 10 times larger than the diameter. The overlapping of ellipsoids orthogonally will reduce the total volume where all components are being measured, slightly increasing the spatial resolution of the measurement. The temporal resolution of an LDV setup is determined primarily by the

concentration of tracing particles and the measurement volume. Unlike HWA or pitot tubes, the sampling rate of LDV is not constant but rather determined by the frequency of particles entering the measurement volume. Higher concentrations increase the probability that at least one particle is present in the measurement volume. However, the presence of more than one particle in the volume at a time reduces the quality of measured signals and presents error when processing the signal. Ideal concentrations of particles place only one in the measurement volume at a time. Reducing the measurement volume itself can also increase the probability that only one particle is present [2].

2.4. Particle Image Velocimetry

Particle Image Velocimetry (PIV) is a popular flow diagnostic technique that allows for the quantitative analysis of entire velocity vector fields within a defined test area or volume. PIV operates by seeding a test region with particles that are illuminated by a high-power laser. PIV cameras take photos in quick succession, up to sub-microseconds, while the laser pulses are synchronized in time with each photo. The light pulses illuminate the test region, reflecting light off of the seeding particles which is detected by the cameras. The resulting photos are compared using cross-correlation techniques which determine the displacement of particles in defined interrogation areas based on pixel intensity distributions. The displacement of each particle divided by the time between photos results in the velocity vector field of the geometry. PIV has seen widespread use over the past two decades due to its ability to accurately measure velocity components over a defined area rather than just at a single point [8]. This allows for better analysis of turbulent flow fields as velocity gradients can be determined and coherent flow structures can be examined, analysis that can’t be done with point measurement techniques such as LDV or HWA.

Typical PIV setups require the use of proper tracing particles, high-power Nd:YAG pulsed lasers, high resolution CCD or CMOS cameras, and image processing software. Choice of seeding particle will be described in further detail in the next section, but unlike LDV, particles must be distributed homogenously throughout the entire test region rather than passing through a single point [2]. A particle seeding apparatus is placed upstream of the flow and disperses a chosen seeding material into the fluid with a desired particle density. This seeding apparatus must be in a proper position to allow particles to be fully dispersed into the test section without interrupting upstream flow that may affect the flow conditions in the test section. The particles are illuminated by a high-power pulse from a Nd:YAG laser as seen in figure 7 with a pulse time of around 5-15 ns. Lasers are chosen for illuminating the particles due to their high intensity and ability to be pulsed quickly, a requirement to reduce the probability of blurry images. To create a laser sheet capable of illuminating the required test section, the beam is passed through a cylindrical lens which expands the beam. Images of the illuminated particles are taken using a high-resolution CCD camera facing the test plane. These images are taken in time with the Nd:YAG laser pulses and the time delay between these images depends on the velocity of the flow region being analyzed, with higher velocity flows requiring higher pulse frequencies [9].

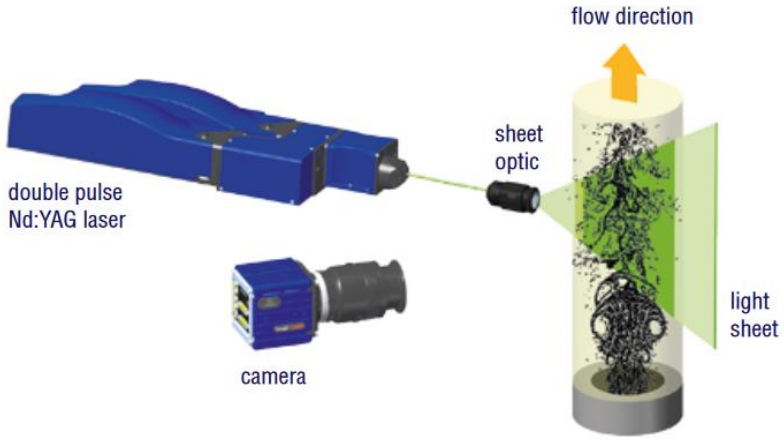

Figure 7. General PIV layout with a dual pulse Nd:YAG laser and single camera [10]

Alternatively, a two-camera setup can be utilized to provide limited 3D analysis of a flow field. Known as stereographic PIV, two cameras are set up at slightly different viewing angles to the flow region and each takes two photos at slightly different times of that region. These images can be similarly compared as described above, but due to their slightly different viewing angles, a small distance in the normal direction of the flow plane can also be visualized and vector components can be calculated as shown in figure 8 [11].

3D PIV, also known as Tomographic PIV, utilizes the same basic principles as 2D PIV, but the overall setup is slightly altered in order to capture all three velocity components of the fluid flow in the analyzed volume. A 4-camera setup is utilized so volumetric components of the test region, or voxels, can be analyzed and used to determine particle locations rather than just the pixel illumination in 2D PIV. Figure 9 shows the general camera setup used in 3D PIV. The entire volume of the test region also must be illuminated by the pulsed laser rather than a 2D sheet [11].

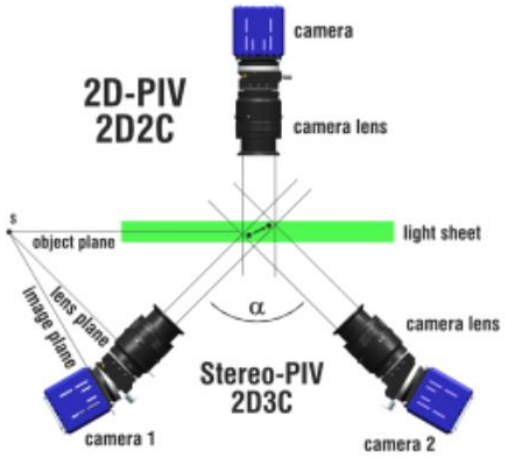

Figure 8. Camera setup of stereographic PIV [10]

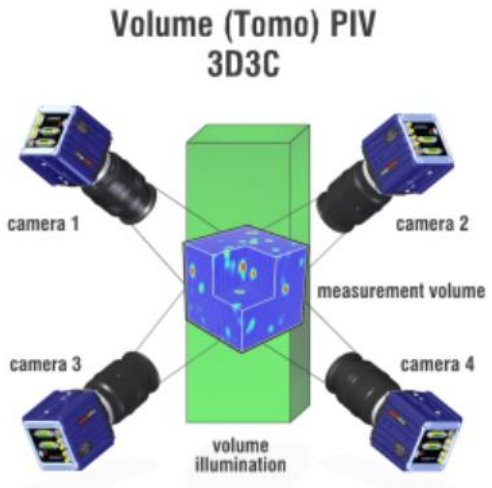

Figure 9. Camera setup of tomographic PIV [12]

Image processing techniques used in PIV analysis are able to determine with high accuracy and precision the average displacement of particles in small interrogation areas of the given photographs. With on average 10^4 interrogations per image, each interrogation area ideally contains 10 or more particles. Because the exact displacement of each particle between frames is not discernable at concentrations this high, spatial cross-correlation analysis of the interrogation areas is required. Ideal results from cross-correlation give an easily discernable displacement-correlation peak which represents the local particle displacement inside the interrogation area. However, several parameters impact the accuracy of cross-correlation, namely particles image pairs in an interrogation area, in-plane motion, out-of-plane motion, and velocity gradients within the area. As stated, 10 or more particle pairs should be present in each interrogation area as increased density of particles increases the peak correlation amplitude. Increases in in-plane motion, or motion of particles in the same plane as the laser sheet, reduces correlation amplitude as particles fail to remain in both interrogation images. Similarly, for out of plane motion, or motion normal to the laser sheet, loss of image pairs reduces correlation amplitude. The presence of a velocity gradient within the interrogation area not only reduces the correlation peak, but the

width of the peak widens, reducing the precision of the cross-correlation as well. Generally, in and out-of-plane motion less than ¼ the size of the interrogation window dimension and laser sheet thickness, respectively, and differences in particle displacement less than the diameter of a particle will result in 95% of interrogation windows producing the correct image displacement. Further improvements of the cross-correlation method and interrogation window analysis can be done, such as subpixel interpolation, window shifting, and multi-grid analysis to reduce erroneous displacements.

2.4.1. Particle Seeding

Seeding techniques and choice of seeding particles is an essential step for successful application of both LDV and PIV as proper particles must be chosen to ensure the flow field is being accurately followed by said particles as well as reflecting enough light to be detected by chosen sensors. The method of inserting seeding particles into a flow field is also important to create a dense enough collection of particles for required temporal or spatial resolution of the flow velocity. The size of tracing particles impacts the ability of particles to accurately follow velocity fluctuations as well as how well light is reflected off of the particle. Optimization is required when choosing tracing particles to balance accuracy of tracking in particular flow phenomena and the illumination requirements [13].

For suspension in gas flows, tracing particles will typically have a diameter, d_p, in the range of 1-10 μm. The small length scales of these particles, which are assumed to be approximately spherical in shape, will result in a very low Reynold's number over the particle. Reynold's number flows less than one are considered in the regime of Stokes' flow or creeping flow. This type of flow is dominated by viscous forces of the fluid and the drag force, F, experienced by a spherical object in this flow regime is expressed in equation 12.

$$F = 3\pi\mu_f d_p U_p \tag{12}$$

Where μ_f is fluid dynamic viscosity and U_p particle velocity. The total force balance of a particle suspended in a gas flow with a density ratio of the particle and fluid much larger than one can be simplified as equation 13 below, with ρ_p representing the density of the tracing particle. $\hat{V}$ on the right-hand side of this equation is the particle lag, or the difference between the particle velocity and the true fluid velocity [13].

$$\frac{\pi d_p^3}{6}\rho_p \frac{dU_P}{dt} = 3\pi\mu_f d_p \hat{V} \tag{13}$$

Rearrangement of equation 13 can be done to find the time constant or frequency response of the particle being used. Equations 14 and 15 show the process of deriving the variable 'C' which corresponds to the frequency response, and its inverse which is represented as τ_p, the time constant or relaxation time of a particle. This time constant is how long it takes a particle of a specific size and density to return to the true flow velocity of the gas it is suspended in. For applications in supersonic or hypersonic flow, the Knudsen number, Kn, must be applied to the relaxation time. A corrected form of τ_p in this flow regime is shown in equation 15 [2].

$$\frac{\pi d_p^3}{6}\rho_p \frac{d\widehat{U_p}}{dt} = 3\pi\mu_f d_p \hat{V} \;\rightarrow\; \frac{d\widehat{U_p}}{dt} = -C\hat{V} \;\rightarrow C = \frac{18\mu_f}{\rho_p d_p^2} \tag{14}$$

$$\frac{1}{C} = \tau_p = \frac{\rho_p d_p^2}{18\mu_f} \rightarrow \tau_p = \frac{\rho_p d_p^2}{18\mu_f}(1 + Kn) \tag{15}$$

A simple determination of how well a tracing particle will follow a particular flow field can be done using Stokes' Number, St, as shown in equation 16. This ratio relates the particle relaxation time with the flow fluctuations of the fluid being analyzed, τf. Most practical

applications require a Stokes' number of less than .1, this results in minimal error of flow tracking. Besides tracking capability, safety and contamination effects of the tracing particles must be considered. Hazardous materials are typically avoided in PIV and LDV applications to avoid harm to researchers. Residue left by tracing particles can impact testing by blocking light exposure of a test section due to particle build up on the test section walls, so use of self-cleaning or evaporating materials is ideal for repeated experimentation [13].

$$St = \frac{\tau_P}{\tau_f} < 0.1 \quad \textbf{(16)}$$

3. DENSITY DIAGNOSTIC TECHNIQUES

Schlieren and Shadowgraph photography is a primarily qualitative visual fluid diagnostics technique that allows for variations in density of a fluid to be visualized. These two methods work on the premise that density changes in a fluid cause a change in the refractive index. This change in refractive index causes fluctuations of the light intensity, which are visualized as shadows by the detecting camera. By shining a light onto a fluid with varying density, the density gradients can be visualized in this manner. This technique is commonly used for identification of shock formations in supersonic and hypersonic flows as shocks are easily identifiable based on their abrupt change in density for compressible fluids. The large density gradients in turbulent flow fields as well as smaller density gradients in lower speed flow and temperature density variations are also capable of being visualized by shadowgraph and schlieren imaging.

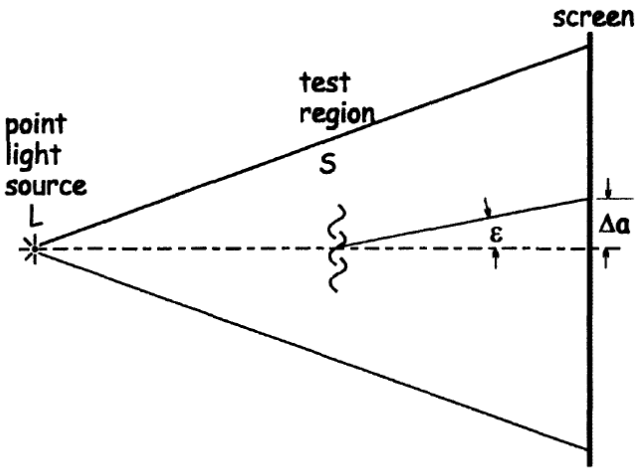

Figure 10. Bending of point source rays due to density gradient [14]

The index of refraction of a particular material is defined as the ratio between the speed of light in a vacuum and the speed of light through the medium. Light travelling through a medium is slightly slowed down due to interaction with the medium's atoms which causes the

light to refract from the original incident ray angle, θ_1. The refraction angle, θ_2, of a beam can be found using Snell's Law as shown in equation 17, in which the index of refraction, n, of both the incident and refracting materials affect the refracted angle relative to the perpendicular of the refracting surface [14].

$$n_1 \sin\theta_1 = n_2 \sin\theta_2 \tag{17}$$

The Gladstone-Dale relation can be used to linearly relate the index of refraction of a gas to its density, shown in equation 18. The K term is the Gladstone-Dale coefficient and is about .23cm^3/g in air. This is the underlying relation for all shadowgraph and schlieren imaging as it shows that changes in a gas's density will impact the refractive index and thus refraction angle of light travelling through the gas [14].

$$n - 1 = K\rho \tag{18}$$

The refraction of light rays past the refracting medium is proportional to the gradient of the index of refraction in the normal plane of the incident light. The actual deflection angle, ε, of the beams is shown in equation 19 [14].

$$\varepsilon = \frac{1}{n}\int \frac{\partial n}{\partial x}\partial z \tag{19}$$

3.1. Shadowgraphs

The method and setup of shadowgraph imaging is very simple and offers an easy way to visualize large density gradients in a test region. Direct shadowgraph imaging setups typically collimate the light beam being used through use of a parabolic lens or mirror. A point source of light is shone onto the apparatus at its focal point to collimate the light beams, and that light is then shined through a density gradient and onto a screen. As shown in figure 10, bent light will

result in shadows to appear on the projection where the density gradient is high. For shadowgraphs specifically, the relative change in light intensity, I, depends on the second derivative of the index of refraction rather than just the gradient, as shown in equation 20, with n_o being the refractive index of the surrounding medium and L being the distance from the test region to the reference plane. While high density gradient flows such as shock waves will be visible with this method, near linear density gradients will become less visible, such as expansion fans and gradients due to temperature fluctuations.

$$\frac{\Delta I}{I} = \frac{L}{n_o}\int \frac{\partial^2 n}{\partial y^2}\partial z \tag{20}$$

3.2. Schlieren Imaging

Schlieren setups, a basic diagram of which is shown in figure 11, are slightly more involved compared to shadowgraph imaging but resulting images are sharper and are capable of visualizing less extreme density gradients. Similar to direct shadowgraph imaging, Schlieren setups collimate a light source with a parabolic lens or mirror and shine the parallel beams through a test region. The resulting beams are then refocused using a second parabolic mirror or lens rather than projected directly onto a screen. At the focal point, a razor edge is placed just close enough to the focal point as to not block any unbent beams of light. This edge does, however, block some light that was bent due to density gradients while allowing other bent beams to shine onto the camera lens or projected screen. This will result in relative light intensity variations on the projected image corresponding to density gradients of the flow similar to shadowgraphs, but with a higher sensitivity to lower gradients as the relative light intensity is related to gradient of the refractive index rather than the second derivative as in shadowgraph

imaging. This higher sensitivity allows for the optical analysis of density gradients invisible to shadowgraph imaging, such as expansion fans and temperature induced gradients [15].

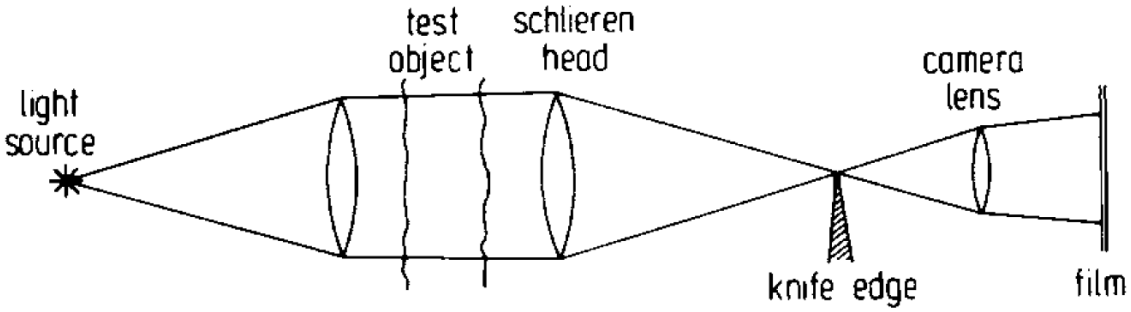

Figure 11. Schlieren setup using parabolic lenses [15]

A laboratory setup of Schlieren imaging used at NDSU can be seen in figure 12. This particular setup utilized two parabolic lenses with focal lengths of 30cm and 60cm, respectively, to collimate and refocus the light at the razors edge. A CCD camera then recorded the resulting image as light passed through the test region consisting of oblique shock waves exiting a supersonic nozzle. The shocks are clearly visible in figure 13, with the light and dark regions corresponding to their locations.

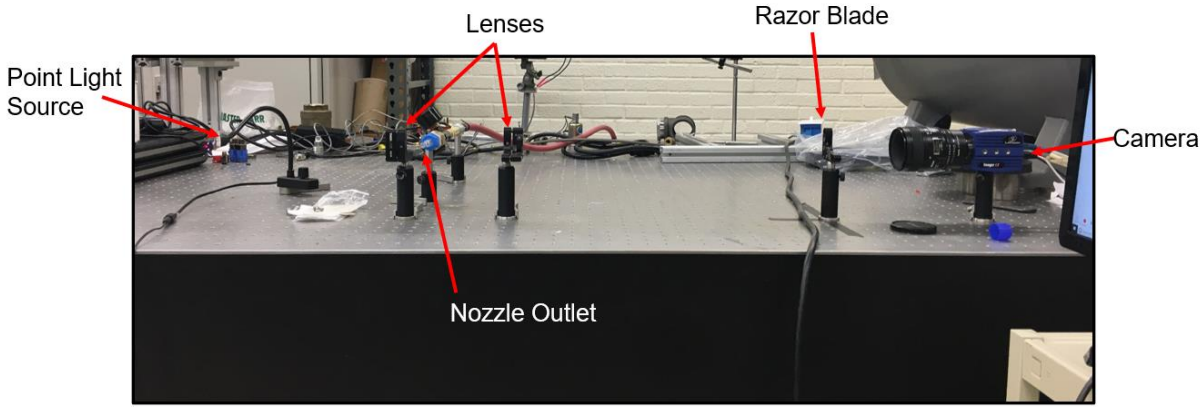

Figure 12. NDSU laboratory setup of a schlieren imaging system
REF: Picture by Matthewscott Dale

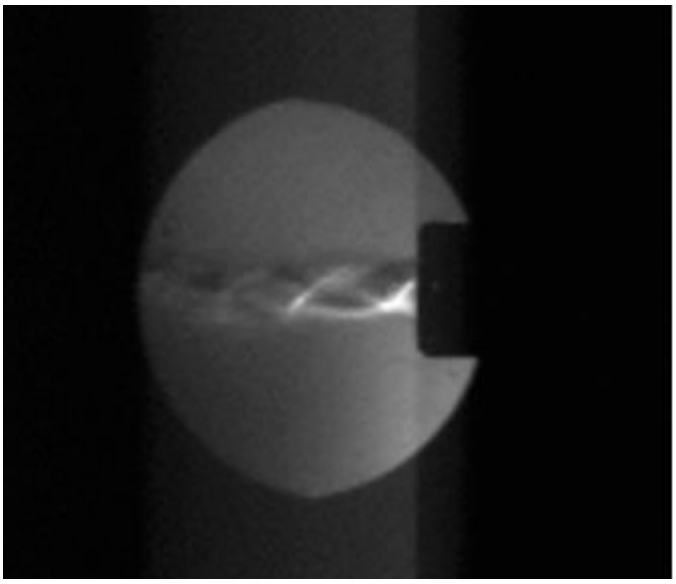

Figure 13. Schlieren image of oblique shock interactions at exit of supersonic nozzle
REF: Picture by Matthewscott Dale

4. PRESSURE AND TEMPERATURE DIAGNOSTIC TECHNIQUES

4.1. Pressure/Temperature Sensitive Paint

Temperature Sensitive Paint (TSP) and Pressure Sensitive Paint (PSP) are polymer-based coatings that are capable of visualizing and giving quantitative measurements of the pressure and temperature distributions on a coated surface by changing the luminescence of the particular paint material. Both PSP and TSP function by utilizing luminescent molecules and combining them with a polymer coating. Certain wavelengths of light will excite the luminescent molecules, causing them to emit light of a longer wavelength which is measured and calibrated to determine the actual pressure and temperature on a given surface. This is a less intrusive diagnostic technique that allows for high-frequency quantitative analysis of pressure and temperature changes on a body. TSP and PSP have wide applications within aerodynamic research with the capability to measure pressure and temperature of the entire body of an aerodynamic object in wind tunnel testing, rather than point-wise measurement of these properties using pressure taps or thermocouples. This allows for more accurate analysis of boundary layer transition effects, force distribution, and validating of CFD simulations [16].

Luminescent dyes excited by a frequency of light will absorb photons and the lumiphores will be excited from their ground states to an excited state. The excitation wavelength of light is specific to the dye being used, but typically ranges from 340 nm (UV) to 450 nm [2]. These lumiphores will then return to their ground states through either a radiationless or radiative process. Radiative processes will emit light with a longer wavelength than the excitation light and this luminescence can be detected by the chosen light sensors. Radiationless processes are often caused by external conversion of the excited lumiphore state through interaction with the system. In the case of PSP, collision with oxygen molecules causes a reduction in the energy

state without the release of a photon, known as oxygen quenching. For TSP, the increase in collision frequency caused by increased temperatures around the paint causes radiationless reduction of the energy state, known as thermal quenching. These two processes reduce the total luminescence of a paint as the oxygen concentration (pressure) and/or temperature increases. The concentration of the dye molecules within the paint needs to be balanced as low concentrations will produce weak signals while too high concentrations risk self-quenching, also reducing the total signal strength. Typical lumiphore materials used for PSP/TSP applications include palladium and platinum porphyrins as well as ruthenium complexes [17].

Binders must also be chosen to allow for successful data collection from PSP/TSP. Binders are ideally stable and safe to apply to a model during the application process. The binder should also be aerodynamically smooth to reduce surface roughness and affect as little as possible the flow conditions of the test model. For PSP in particular, the binder must be oxygen permeable to allow for the dye molecules to be quenched by the presence of oxygen before the lumiphores return to their ground state. TSP binders are chosen with oxygen impermeability to reduce quenching effects to just the thermal quenching process. For PSP, dimethylsiloxane polymers are commonly used due to their oxygen permeability while TSP is capable of using conventional binders such as polyurethane [18].

A light source with stable intensity within the excitation range of the chose luminous dye is required for accurate and consistent PSP/TSP measurements. Fluctuations of the source light intensity cause significant luminosity fluctuations and can be a major source of error. Many commercial PSP/TSP formulations utilize dyes with excitation ranges in the visible spectrum, allowing for the use of LED arrays to illuminate the required test models. LEDs are ideal light sources as they are cheap, easy to set up, and small. Detection of the light intensity fluctuations is

typically collected using CCD cameras with high resolutions in order to detect small pressure fluctuations accurately and precisely. A simplified experimental setup for PSP is shown in figure 14.

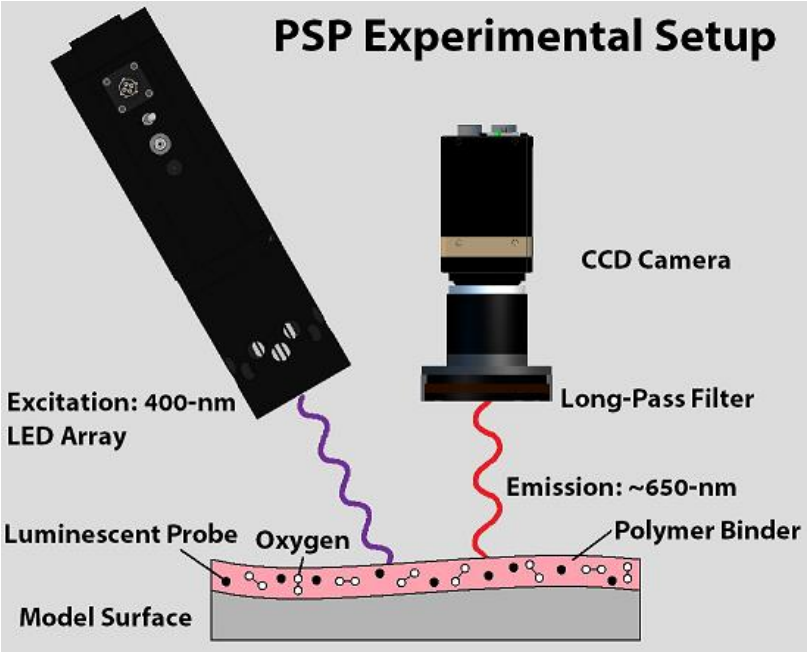

Figure 14. General experimental setup for PSP [19]

Temporal ranges of PSP/TSP can vary, but proper formulations will often give response times in the range of milliseconds, such as "Turbo" PSP [19]. For PSP, as pressure fluctuations increase, the thickness of paint being quenched decreases, resulting in lower signal strength but fluctuations are still measurable. Fluctuations with less than a 1ms response time can be detected by a PSP layer as thin as 5 μm. For TSP, the response time of thermal quenching is much lower than the rate of thermal diffusion at the boundary, resulting in response times ranging from 5-20 ms. Fast 'porous' paints have also been formulated that free the oxygen within the surface paint pores to allow fast responses, in the order of 20 kHz, and provide instantaneous data in high frequency environments [19]. To minimize the error from light intensity and paint thickness variations, wind-off (no-flow) and wind-on are taken and ratioed to remove the uncertainty

associated with those factors' variability. Also, it is noted that these paints are not capable of withstanding high temperatures so their applications are for relatively cold environments.

4.2. Infrared Thermometry

Infrared thermography is a temperature measurement method that utilizes thermal cameras to detect the infrared radiation (IR) being emitted from a body and determine its true temperature. All objects above absolute zero emit wavelengths of light due to that object's temperature. An idealized black body will emit the highest intensity of this radiation at a particular temperature, and the range of electromagnetic radiation emitted is a continuous frequency spectrum that is defined using Planck's Law. The spectral radiance peaks at a particular wavelength depending on the body temperature, and as a body increases its temperature, the peak wavelength emitted decreases in length. For bodies with a temperature lower than 2000 K, the primary wavelengths of light being emitted are in the IR spectrum and require thermal imaging equipment to detect this radiation. The temperature can be determined from the wavelengths emitted if accurate values of emissivity, surrounding temperature, as well as the effective atmospheric transmittance, but more common research techniques utilize in-situ calibration for higher accuracy [20]. The high spatial resolution of infrared thermography as well as its complete non-intrusiveness to the flow allows for accurate and even time resolved analysis of temperature distributions on a surface. Knowledge of thermal distribution can assist in finding many quantities of a flow field, such as thermal boundary conditions and surface heat transfer coefficients [2].

In situ calibration of thermographic cameras works by calibrating the images with measured surface temperatures using thermocouples placed around the measured body. With the locations of the thermocouples known, the temperatures at these points can be correlated with the

IR waves detected, allowing for temperature around the thermocouple to be approximated as well using this calibration. This method of calibration is easier and more commonly used in research and industry as proper measurement or estimation of the myriad of factors that can affect the wavelengths emitted from a surface makes analytical solutions for the temperature difficult [2]. However, the accuracy of in situ calibration depends not only on the camera equipment used to image the flow, but the thermocouple accuracy must also be considered, both in its calibration procedure as well as any affect it may have on the flow dynamics on the body surface. The temporal resolution is primarily limited by the frame rate of the camera used, with most infrared cameras operating in the 30-60 Hz range.

As mentioned, infrared thermography allows for the determination of many flow parameters dependent on surface temperature distributions, namely heat transfer coefficients as well as thermal boundary conditions. Proper measurement and deduction of these parameters also allows for the verification of CFD simulations and the thermal distributions estimated with them. Airfoils and turbomachinery are common bodies examined using infrared thermography, but emissivity changes, combustion, and other chemical reactions in the test region can significantly impact the accuracy of temperature measurements.

5. CONCLUSION

The multitude of diagnostic techniques available to fluid dynamics researchers allows for the accurate analysis of velocity, density, temperature, and pressure distributions on and around objects in a flow field. Techniques such as pitot tubes and HWA allow for analysis of velocity at a point, but the intrusive nature of these probes can have significant effects on the flow dynamics of a system. Alternative techniques like LDV and PIV allow for point wise and area/volume analysis of the velocity component, respectively, but require high powered lasers and deliberate choice of seeding materials to accurately measure the flow velocity. PIV in particular has proven to be one of the most popular and widely used velocimetry techniques due to its ability to visualize flow over an area rather than just at a point, making it very useful in analyzing velocity gradients especially in turbulent flow. Shadowgraph and schlieren imaging provide simple techniques for visualizing the second and first order derivatives of the density gradient in a test section, respectively, and are of particular use for visualizing shock wave formations. PSP provides high spatial resolution alternative to pressure taps on a body to measure surface pressure and is invaluable for determining loads on a model as well as for confirming the accuracy of CFD codes. TSP and infrared thermography are both high spatial resolution temperature measurement techniques that gives an alternative to the use of just thermocouple probes. While this paper reviews only a small sample of some of the more common diagnostic experimentation methods used by researchers and in industry, the fundamental principles of these techniques have been and continue to be improved on to more precisely and accurately measure complex flow phenomena.

REFERENCES

[1] J. D. Anderson, *Modern Compressible Flow: With Historical Perspective*, 3rd ed. New York, NY, USA: McGraw-Hill, 2003.

[2] *Springer Handbook of Experimental Fluid Mechanics*, Berlin, Brandenburg, Germany: Springer, 2007.

[3] P. C. Stainback and K. A. Nagabushana, "Review of hot-wire anemometry techniques and the range of their applicability for various flows," *Electronic Journal of Fluids Engineering*, 1993.

[4] G. Comte-Bellot, "Hot-wire anemometry," *Annual Review of Fluid Mechanics*, vol. 8, no. 1, pp. 209-231, 1976, doi: 10.1146/annurev.fl.08.010176.001233.

[5] H. H. Bruun, *Hot-Wire Anemometry: Principles and Signal Analysis*, New York, NY, USA: Oxford University Press, 1995.

[6] F. Mayinger, *Optical Measurements: Techniques and Applications*, New York, NY, USA: Springer, 1994.

[7] L. E. Drain, *The Laser Doppler Techniques*, New York, NY, USA: John Wiley & Sons, 1980.

[8] M. Raffel, C. E. Willert, and J. Kompenhans, *Particle Image Velocimetry: a Practical Guide*, vol. 2, 3rd ed. Berlin, Brandenburg, Germany: Springer, 2018.

[9] R. J. Adrian, "Twenty years of particle image velocimetry," *Experiments in Fluids*, vol. 39, pp. 159-169, 2005, doi: 10.1007/s00348-005-0991-7.

[10] "2D and stereo PIV." LaVision. https://lavision.de/en/applications/fluid-mechanics/2d-stereo-piv/index.php (accessed Mar. 15, 2023).

[11] C. E. Willert and M. Gharib, "Digital particle image velocimetry," *Experiments in Fluids*, vol. 10, no. 4, pp. 181-193, 1991, doi: 10.1007/BF00190388.

[12] "Tomographic PIV." LaVision. https://lavision.de/en/applications/fluid-mechanics/volumetric-tomographic-piv/index.php (accessed Mar. 20, 2023).

[13] A. Melling, "Tracer particles and seeding for particle image velocimetry," *Measurement Science and Technology*, vol. 8, pp. 1406-1416, 1997, doi: 10.1088/0957-0233/8/12/005.

[14] G. S. Settles and M. J. Hargather, *Schlieren and Shadowgraph Techniques: Visualizing Phenomena in Transparent Media*, New York, NY, USA: Springer, 2001.

[15] W. Merzkirch, *Techniques of Flow Visualization*, 2nd ed. London, England, UK: Academic Press Inc., 1987.

[16] T. Liu, J. P. Sullivan, K. Asai, C. Klein, and Y. Egami, “Pressure and temperature sensitive paints,” *Encyclopedia of Aerospace Engineering*, vol. 1, 2011, doi: 10.1002/9780470686652.eae076.

[17] A. Vollan and L. Alati, "A new optical pressure measurement system (OPMS)," *ICIASF '91 Record., International Congress on Instrumentation in Aerospace Simulation Facilities*, pp. 10-16, 1991, doi: 10.1109/ICIASF.1991.186219.

[18] F. Rodriguez, C. Cohen, C. K. Ober, and L. Archer, *Principles of Polymer Systems*, 6th ed. New York, NY, USA: McGraw-Hill, 2014.

[19] “Pressure sensitive paint.” ISSI. https://innssi.com/psp/ (accessed Apr. 1, 2023).

[20] G. Gaussorgues and S. Chomet, *Infrared Thermography*, Dordrecht, South Holland, Netherlands: Springer, 1994.